

# We are IntechOpen, the world's leading publisher of Open Access books Built by scientists, for scientists

4,800

Open access books available

122,000

International authors and editors

135M

Downloads

Our authors are among the

154

Countries delivered to

TOP 1%

most cited scientists

12.2%

Contributors from top 500 universities



WEB OF SCIENCE™

Selection of our books indexed in the Book Citation Index  
in Web of Science™ Core Collection (BKCI)

Interested in publishing with us?  
Contact [book.department@intechopen.com](mailto:book.department@intechopen.com)

Numbers displayed above are based on latest data collected.  
For more information visit [www.intechopen.com](http://www.intechopen.com)



# Design of Radial Power Combiners Based on TE<sub>01</sub> Circular Waveguide Mode

*José R. Montejo-Garai, Jorge A. Ruiz-Cruz  
and Jesús M. Rebollar*

## Abstract

Modern microwave and millimeter-wave systems require high-power amplifiers in very diverse fields such as communications or plasma physics. Although amplification technology has significantly evolved in the last decades, a single module is not enough for achieving the required power level. The solution in this case is the combination of several individual modules with power combiners. In this chapter, this concept is shown with two E-plane radial power combiners, both carrying a high-power signal with the circular waveguide TE<sub>01</sub> mode. The first design is a 16-way Ku-band combiner with an excellent experimental performance: return loss better than 30 dB, with a balance for the amplitudes of  $\pm 0.15$  dB and  $\pm 2.5^\circ$  for the phases, in a 16.7% fractional bandwidth (2 GHz centered at 12 GHz), and efficiency better than 95% in this band. The second design is a 5-way W-band combiner, showing excellent characteristics as well: the experimental prototype has a return loss better than 20 dB, with a balance for the amplitudes of  $\pm 0.4$  dB and  $\pm 3.5^\circ$  for the phases, in a 12.8% fractional bandwidth (12 GHz centered at 94 GHz), and efficiency better than 85% in this whole band. The experimental results obtained in both designs are the state of the art in the area of radial power combiners.

**Keywords:** radial combiner, mode transducer, mode conversion purity,  $N$ -way divider/combiner, evanescent mode, propagating modes, higher-order modes, return loss, isolation

## 1. Introduction

There are a large number of high-frequency systems making an extensive use of high-power modules, especially in modern systems at microwave and millimeter wave bands for research, industry and defense. Some of these applications are new communication systems with higher capacity, weather and control radars, space exploration, and scientific facilities for particle accelerators or for plasma physics [1–3]. The high-power modules required in these systems, although they may have very diverse type of specifications, require all typically high efficiency in the power amplification process, with high linearity, and over a wide frequency band. A single individual module is, in many cases, not enough to achieve this high performance in a single stage, and power combination is a classical strategy to overcome this situation. With this strategy, the requirements of the individual amplification modules

are less stringent, simplifying their design, at the expense of introducing a unit for the power combination, which can be done very efficiently, as this chapter will show with two examples.

Amplification at the microwave and millimeter wave bands have been typically based on high power vacuum devices such as klystrons, magnetrons, traveling wave tubes (TWTs), etc. [4]. Although they are still a common solution at some high frequency bands, these devices may suffer from some drawbacks such as their very hard requirements of high-voltage supply, inherent thermionic noise, limited lifetime of the filament, etc. To overcome these issues implies a high cost, especially when the operation frequency increases, and some applications may not afford it.

After a continuous research over last decades, solid-state technology has become an alternative to these vacuum devices. Along with this development, power combination techniques have become crucial, for instance when a solid-state power amplifier (SSPA) module cannot provide enough power. In this case, the power combiner unit (which can be also seen, indistinctly, as a power divider because of the reciprocity for passive waveguide components) becomes a key component, which must have very stringent specifications. It must have very low insertion loss, since it has to deal with high-power signals; a high insertion loss implies less efficiency, but also high-power dissipation and heating of the unit. The different signals must be combined with a very good balance in amplitude and phase. Other important requirements are the return loss level at the input port and the isolation between the output ports.

These varieties of requirements for the power combiner have led to many topologies for implementing this function. The configuration based on a structure with a radial symmetry between the input and output ports has some intrinsic advantages in comparison with the chain-type or corporate-type combiners [5], especially when dealing with a large number of ports [6, 7]. Since the configuration has a radial symmetry, all the paths from the input to the output ports are guaranteed to be equal, providing a perfect amplitude and phase combination from the theoretical point of view (i.e., manufacturing tolerances may slightly degrade this ideal operation).

With respect to the most suitable high-frequency transmission system to implement the combiner, metallic hollow waveguides provide several advantages such as low insertion loss and high power capability. Since waveguides are larger in size in comparison to planar wave guiding structures, they exhibit higher robustness and stability, which are crucial for amplifier modules and plasma heating for fusion energy [8].

Many radial waveguide combiners can be found in the literature for Ku and Ka frequency bands. The work in [9] presents a wideband 60 GHz 16-way power divider with 20% bandwidth and 12 dB return loss level. A 19-way isolated radial combiner is presented in [10], with 12 dB return loss level in a 24.4% bandwidth at 20 GHz. A 24-way radial combiner at Ka band is proposed in [11], with 25 dB return loss level in a 15% bandwidth. A 20-way Ka-band design with 10 dB return loss level is shown in [12] with a 25% bandwidth. The design in [13] shows a very competitive performance, which will be further reviewed in this chapter.

At W-band, power combiners with radial symmetry are not as common as in lower frequency bands. A four-way design, using a corporate scheme implemented in H-plane waveguide configuration is reported in [14], with a T-junction for the division. It has a theoretical return loss (the measurement is carried out in back-to-back configuration) better than 10 dB in an 11.8% fractional bandwidth (96–108 GHz). A four-way waveguide power divider is shown in [15] with a return loss better than 13 dB in a 31.6% fractional bandwidth (80–110 GHz). This design has the output ports with 180° out of phase. A W-band solid-state power amplifier is

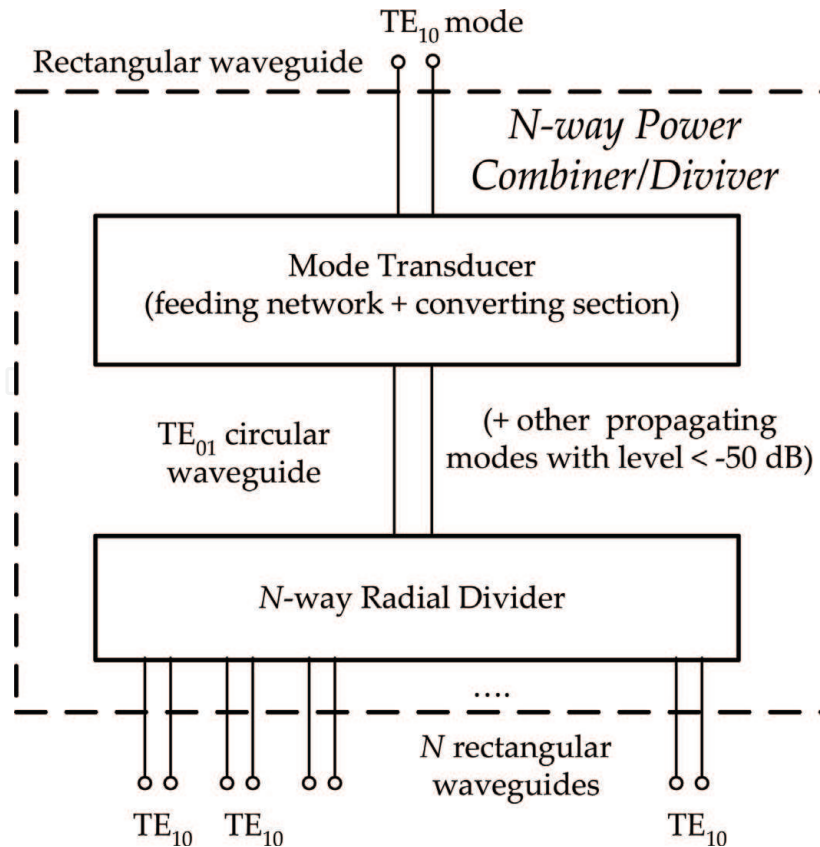


**Figure 1.** Scheme of the radial power combiner (or divider) made up of (i) the mode transducer between the rectangular waveguide  $TE_{10}$  mode and the circular waveguide  $TE_{01}$  mode, and (ii) the  $N$ -way radial divider (or combiner) dividing the power carried by the circular waveguide  $TE_{01}$  mode into  $N$  rectangular waveguide  $TE_{10}$  modes.

presented in [3], using two types of waveguide combiners: a 4-way septum waveguide combiner and a 12-way radial-line waveguide combiner. The 4-way septum waveguide combiner is of the corporate type [5]. The 12-way radial-line waveguide combiner is composed of a transition from rectangular waveguide to coaxial, and then goes into the central radial-line section. Very recently [16], a 5-port W-band design has been proposed. The features of this structure are discussed in this chapter, with additional details related to the ideal S-parameters of the structure guiding the design.

When working with radial power combiners involving circular and rectangular waveguides, as the designs shown in this chapter, two main characteristics will determine the features of the final unit. The first one is the geometry of the mode transducer connected to the divider, which will be directly related to the compactness of the combiner and the level of the excited higher-order modes. The second one is the use of resistive elements or sheets within the structure to improve the isolation between the output ports [17]. In this case, the mechanical design must take into account the integration of the resistive sheets, and the insertion loss level and the power handling are usually degraded. Moreover, the amplitude and phase balance may also get worse.

Taking into account all these considerations, this chapter presents the design of two radial power combiners in waveguide technology. The prime objective has been to obtain competitive designs suitable for manufacturing at microwave and millimeter wave bands, giving priority to the following key requirements: the return loss level at the common input port, the insertion loss from the input to the different outputs, the power handling capability, and the balance of both amplitude and phase between the output ports. It will be emphasized how to control these requirements with a common strategy for designs with different number of ports



and for different frequency bands. Nevertheless, for the final implementation, the different manufacturing technologies have to be taken into account in the final design process, since the control of the dimensions with respect to the tolerances and fabrication strategy (material, cuts of the parts, assembly, etc.) for the different frequency bands is crucial for achieving a successful experimental prototype.

**Figure 1** shows a detailed scheme of the topology used for the two E-plane power combiners [13, 16] discussed in this chapter. It has a mode transducer between the rectangular waveguide  $TE_{10}$  mode and the circular waveguide  $TE_{01}$  mode, and the  $N$ -way radial divider. In this structure, it will be ensured that the other propagating modes, as well as the evanescent modes, have all a level of at least 50 dB lower than the desired circular waveguide  $TE_{01}$  mode just before the radial divider. This is essential to have a broadband performance and for avoiding spurious resonances in the response. The structure will be used for two designs. The first design is a 16-way Ku-band combiner, centered at 12 GHz with 2 GHz of bandwidth (16.7% fractional bandwidth). The second design is a 5-way W-band combiner, centered at 94 GHz with 12 GHz of bandwidth (12.8% fractional bandwidth).

## 2. Design of the circular waveguide $TE_{01}$ mode transducer

### 2.1 Foundation of the mode transducer operation

The radial combiner in **Figure 1** is based on the  $TE_{01}$  circular waveguide mode, which is used in different fields of microwave and millimeter wave engineering. For instance, some oversized circular waveguides work with the  $TE_{01}$  mode because of its low attenuation constant, since its electric field is progressively smaller when approaching the circular boundary [18–19]. Metallic cavities made up of a cylinder with circular cross section provide resonant  $TE_{01p}$  modes, used for microwave filters with very low insertion loss, and this type of cavities are also common in plasma systems, gyrotrons, masers, etc. [20–23].

In all these applications, it is necessary to convert first the power coming from the generator in the fundamental mode of a suitable transmission system (typically a coaxial, or a rectangular waveguide for high frequency bands) into the  $TE_{01}$  circular waveguide mode, which is not the fundamental mode of the circular waveguide. The device performing this function is the circular waveguide  $TE_{01}$  mode transducer. Although there are many implementations of this device, there are two main methods for the generation of this mode from a  $TE_{10}$  rectangular waveguide mode.

The first developed method was based on transforming the cross-section of the input rectangular waveguide progressively into the cross-section of the output circular waveguide, leading to a flared structure. This conversion is usually very long and involves many sections cascaded in-line following a symmetric pattern in order to prevent the generation of higher-order modes, which may degrade the overall performance [11]. Some examples are the Southworth-type converter [18, 24], the Marie-type [25, 26], and the sector converter [27]. At the beginning of these developments, the design of this type of converters was based on the expertise of the designers; nowadays, powerful tools for computer aided design (CAD) are also combined with the know-how of the designers. The main drawbacks of this kind of in-line configuration are their large length and the high level of the excited undesired modes [11].

The second method uses a sidewall coupling (by one or more several sides) between the rectangular and the circular waveguides [28]. The flower-petal transducer follows this configuration [29]. There are two main drawbacks for this

structure, its narrow bandwidth and its high insertion loss level. Ka-band transducers with four branches are presented in [12, 30], showing moderate return loss level. In these references, the sidewall coupling is a simple aperture with limited degrees of freedom. As shown in [31], better return loss and wider band can be obtained by improving the sidewall coupling. Hence, the designs presented in this chapter are based on improvement made to the sidewall coupling.

The work in [31] forms the basis for the designs. **Figure 2** shows the operating principle of this type of transducer. In this figure, the converting section (dashed circle) is excited in its four sides by the  $TE_{10}$  rectangular mode, generating the  $TE_{01}$  mode at the circular waveguide. **Figure 2** also shows the feeding network routing the input to the four arms of the converting section.

For the design of the transducer, the classical goal is to obtain a challenging return loss at the input with high purity conversion to the circular waveguide  $TE_{01}$  mode. Thus, it is essential to control the level of the non-desired modes in the circular waveguide, especially those that are propagating, with lower cutoff frequency than the  $TE_{01}$  mode. A higher level for these modes degrades the conversion efficiency, but it can also lead to spurious resonances in the power divider (not always treated in detail in the literature of these devices). Thus, the first consideration in the design is to identify how the different propagating modes of the circular waveguide can be controlled, since the  $TE_{01}$  mode is not its fundamental mode (i.e., it is not the mode with the lowest cutoff frequency).

This study can be done by analyzing the modes with respect to the number of symmetry planes (1, 2 or 4) of the physical structure along with the symmetry of the excitation, as in **Table 1**. **Table 1** shows the modes associated to the cases of one, two or four symmetry planes and the normalized cut-off frequencies of the modes involved in the structure. The excitation in **Figure 2** will be done with the  $TE_{10}$  mode of the rectangular waveguide at the input, which has electric wall (EW) symmetry. The  $TE_{01}$  mode of the circular waveguide has EW symmetry at four symmetry planes of the circular waveguide, including the planes at the four sides for the excitation. In fact, this  $TE_{01}$  mode has EW symmetry for any radial plane.

The study leads to the following considerations:

- a. The converting-section has four symmetry planes, all with EW boundary condition, including the radial planes crossing the sides of the excitation. Thus, according to the third column of **Table 1**, the only propagating mode in the circular waveguide under this excitation is the  $TE_{01}$ .
- b. The feeding-network has only one physical symmetry plane.
- c. Thus, the complete transducer has only one physical symmetry plane, with EW symmetry boundary condition. Therefore, in the optimization of the final transducer, the amplitudes of the propagating  $TE_{11c}$  and  $TE_{21c}$  modes must be kept under very low levels. The  $TM_{11s}$  and  $TE_{31c}$  modes have also to be controlled for avoiding higher-order mode interactions with the radial divider ( $TM_{21s}$  is under cut-off in the designed bands). This will allow reducing later the length of the circular waveguide connecting the transducer and the radial divider.

## 2.2 Converting section design

The converting section has two symmetry planes with four rectangular ports at the excitation sides. This avoids the generation of the  $TE_{21c}$  mode, according to the considerations in previous subsection. In addition, some kind of matching elements must be included for obtaining a challenging return loss level in broadband

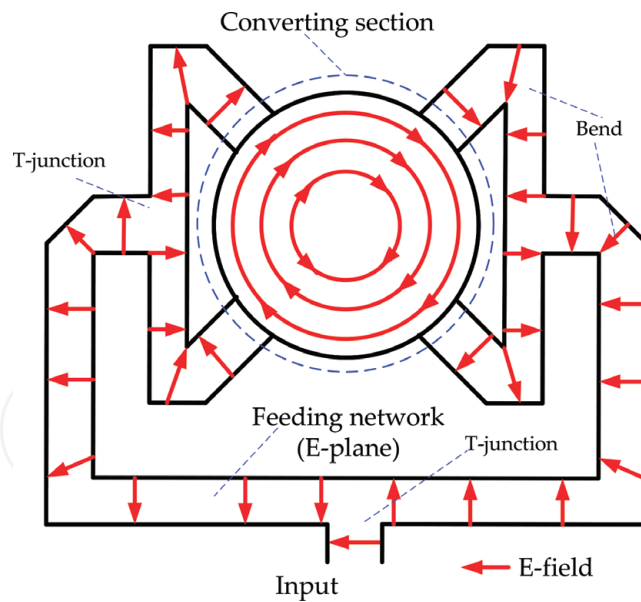


**Figure 2.** Scheme of a sidewall coupling for a circular waveguide  $TE_{01}$  mode transducer, showing the electric field lines, the converting-section (dashed circle) excited in its four sides, and the input feeding network (with E-plane T-junctions and waveguide bends).

Circular waveguide modes excited under different field symmetry planes			
All modes $k = \frac{f_c}{f_{cTE_{nl}}}$	One symmetry plane electric wall (EW)	Two symmetry planes electric wall (EW)	Four symmetry planes electric wall (EW)
$TE_{11c} \ k = 1$			
$TE_{11s} \ k = 1$			
$TM_{01} \ k = 1.31$			
$TE_{21c} \ k = 1.66$	$TE_{21c}$	$TE_{21c}$	
$TE_{21s} \ k = 1.66$			
<b><math>TE_{01} \ k = 2.08</math></b>	<b><math>TE_{01}</math></b>	<b><math>TE_{01}</math></b>	<b><math>TE_{01}</math></b>
$TM_{11c} \ k = 2.08$			
$TM_{11s} \ k = 2.08$	$TM_{11s}$		
$TE_{31c} \ k = 2.28$	$TE_{31c}$		
$TE_{31s} \ k = 2.28$			
$TM_{21c} \ k = 2.79$			
$TM_{21s} \ k = 2.79$	$TM_{21s}$	$TM_{21s}$	

*In boldface, the highlighted circular  $TE_{01}$  mode is used to connect the mode transducer with the N-way radial divider.*

**Table 1.** Circular waveguide modes associated to the case of one, two, or four symmetry planes and their normalized cut-off frequencies.

applications. This is done with a one-section stepped transformer shown in the insets of **Figure 3a** and **b**, connecting the circular waveguide with the rectangular waveguide ports. A circular metallic post has been also placed at the bottom of the cylinder for improving the return loss.

**Figure 3** shows the simulated response of the converting-section for both designs at Ku- and W-band, respectively, obtained with CST Microwave Studio [32]. The simulations have taken into account the four symmetry planes. In both designs, the return loss level for the  $TE_{01}$  mode is better than 30 dB. In the insets of **Figure 3**, a 3D CAD view of the final converting section is included.

It is important to note that, in this structure, the only propagating mode at the circular waveguide is the  $TE_{01}$ , according to the third column of **Table 1**, and, thus, the reflection coefficient in **Figure 3** fully characterizes the behavior of the converting section with the considered symmetries. Moreover, it is also emphasized that the manufacturing process has been taken into account in the full-wave optimization, imposing constraints and limitations in the dimensions of the matching elements for easing the fabrication. For instance, for the W-band design that will be implemented by micromachining, corners are rounded in the simulation with 0.2 mm radius. In addition, the transformer sections keep the width of the WR10 standard waveguide used for the ports.

### 2.3 Feeding network design

The converting section is fed from the input rectangular port by means of the feeding network shown in **Figure 2**, which is composed of the following building blocks: two types of T-junctions and three types of waveguide bends, all in E-plane configuration (there is no width variation in the feeding network).

All these individual components (the building blocks), and their connection (leading to more complex building blocks), must preserve the bandwidth and the return loss level obtained previously in the converting section. Moreover, the footprint is minimized. A step-by-step process has been carried out in the design of all these individual components separately. The complete feeding network is obtained after a final optimization, varying only some connection lengths between its building blocks.

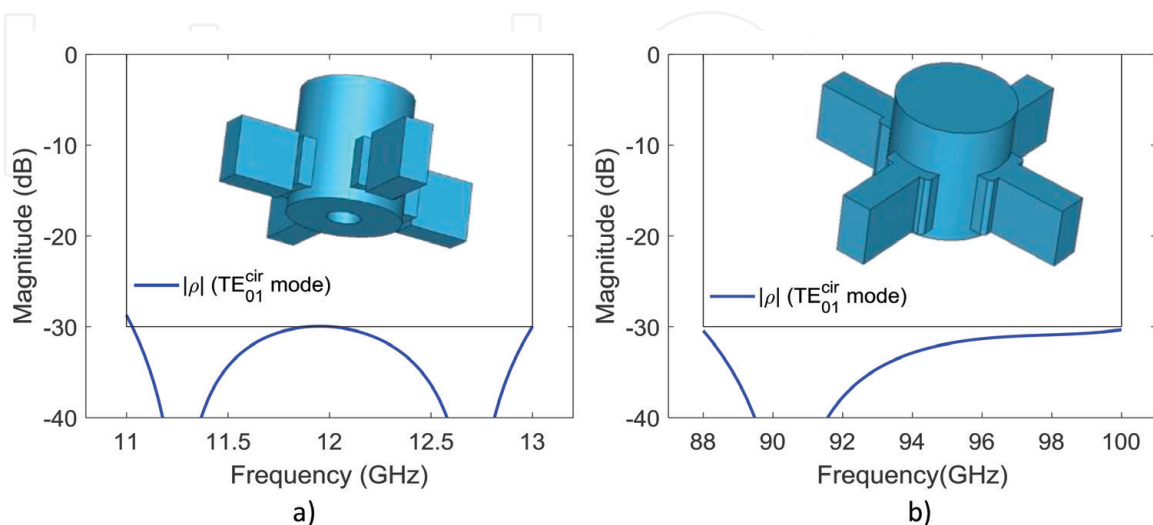


**Figure 3.** Simulated response of the reflection coefficient for circular waveguide  $TE_{01}$  mode in the converting-section, taking into account the four symmetry planes with electric wall boundary condition (EW). In the insets, a 3D CAD view of the full converting-sections is shown. (a) Ku-band response and (b) W-band response.



## 2.4 Final design of the transducer

The converting section and the feeding network, separately designed in the previous stages, are now connected. A final optimization is carried out in order to fulfill the specifications of the return loss level and high purity conversion from the rectangular waveguide  $TE_{10}$  mode to the circular waveguide  $TE_{01}$  mode. Only one-half of the converter is analyzed due to the single physical symmetry plane of the complete transducer, which has EW field symmetry. This reduces the time of the full-wave simulations. Nevertheless, since accurate results are needed in this stage, the high computational cost of the electromagnetic analyses makes crucial to minimize the number of optimization variables.

In addition, the cost function, which traditionally only involves the return loss and/or the insertion loss, must also include the level of the four higher propagating modes in the circular waveguide ( $TE_{11c}$ ,  $TE_{21c}$ ,  $TM_{11s}$ ,  $TE_{31c}$ , according to the first column of **Table 1**), for controlling their required attenuation with respect to the desired  $TE_{01}$  mode. As it could be expected, the radius of the circular waveguide is a key optimization parameter, since it controls the cutoff frequency of the modes, and it is directly related to the challenging level of 30 dB required for the return loss.

The final structure of the transducer in Ku-band is presented in the inset of **Figure 4a**, where the electric field pattern under operation is also shown. **Figure 4a** shows the simulated response achieving a return loss level higher than 30 dB, while **Figure 4b** shows the attenuation level, higher than 50 dB, for the four propagating modes in the design band from 11 to 13 GHz. A back-to-back measurement of two similar transducers manufactured in brass can be seen in [13], showing a very good agreement with respect to the theoretical simulation.

The final mode transducer for the W-band design is shown in the inset of **Figure 5a**, also with the electric field configuration. The simulated return loss, with a level better than the specified 30 dB, is shown in **Figure 5a**. The response for the attenuation is shown in **Figure 5b**, achieving levels higher than 55 dB for the four propagating modes in the design band from 88 to 100 GHz.

Both transducers have been designed in this chapter for integration with a radial divider. However, they can be also used as separated devices in diverse applications of high-energy particle accelerators or plasma heating. In all these cases, power rating is a key parameter. For the presented transducers, it has been calculated at the lowest frequency of operation in each band, i.e., 11 GHz in Ku-band and 88 GHz

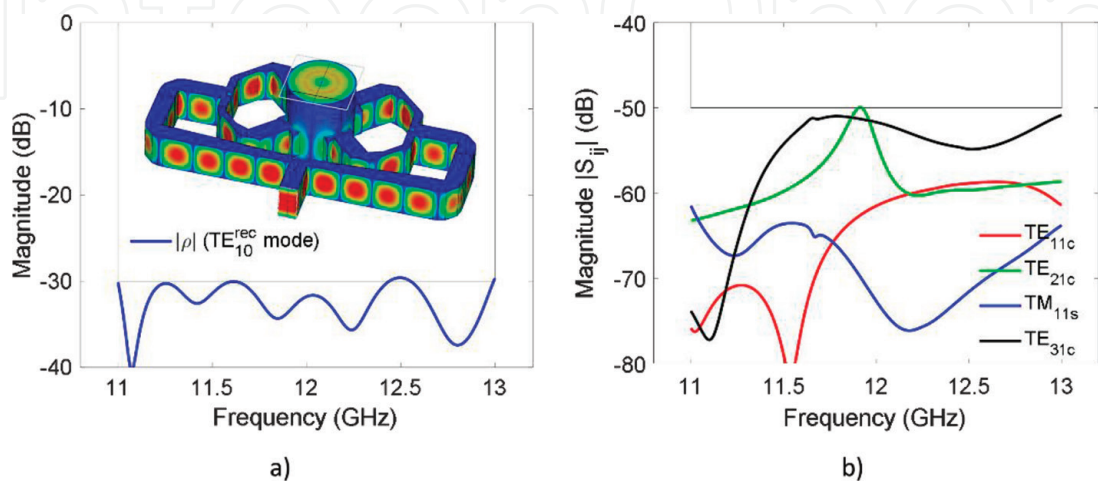


**Figure 4.**

(a) Simulated return loss of the Ku-band transducer, better than the 30 dB goal in 2 GHz centered at  $f = 12$  GHz (16.7%). In the inset, the electric field configuration is shown. (b) Level of the four propagating modes (transducer with one physical symmetry plane having EW) at the circular waveguide (transmission from  $TE_{10}^{rec}$ ), higher than 50 dB in the 11–13 GHz band.

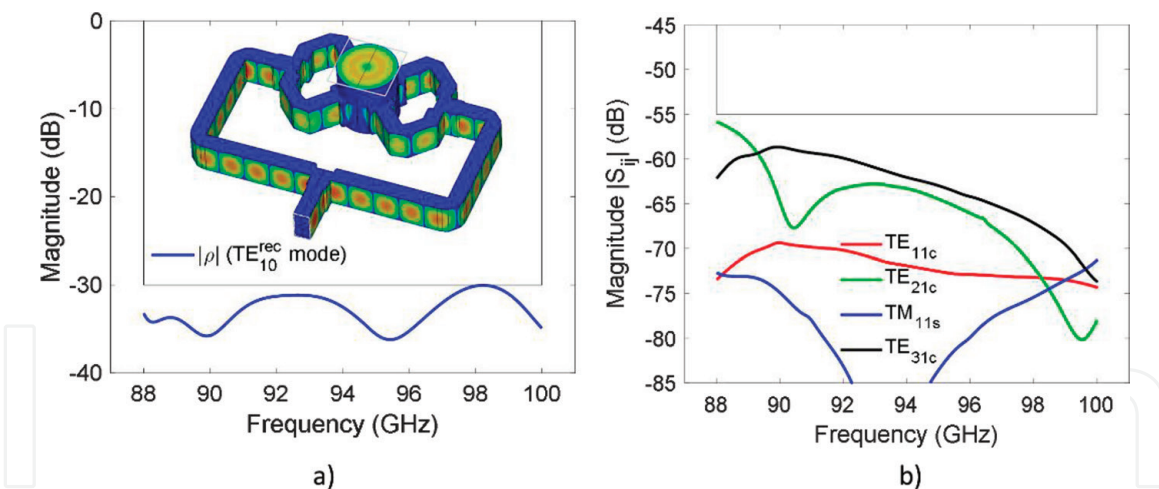


**Figure 5.** (a) Simulated return loss of the W-band transducer, better than the 30 dB goal in 12 GHz centered at  $f = 94$  GHz (12.8%). In the inset, the electric field configuration is shown. b) Level of the four propagating modes (transducer with one physical symmetry plane having EW) at the circular waveguide (transmission from  $TE_{10}^{rec}$ ), higher than 55 dB in the 88–100 GHz band.

in W-band. Assuming a break down field of 30 kV/cm, and analyzing the critical dimension of each design, a 240 kW value has been obtained for the Ku-band transducer, while 9.6 kW for the W-band design.

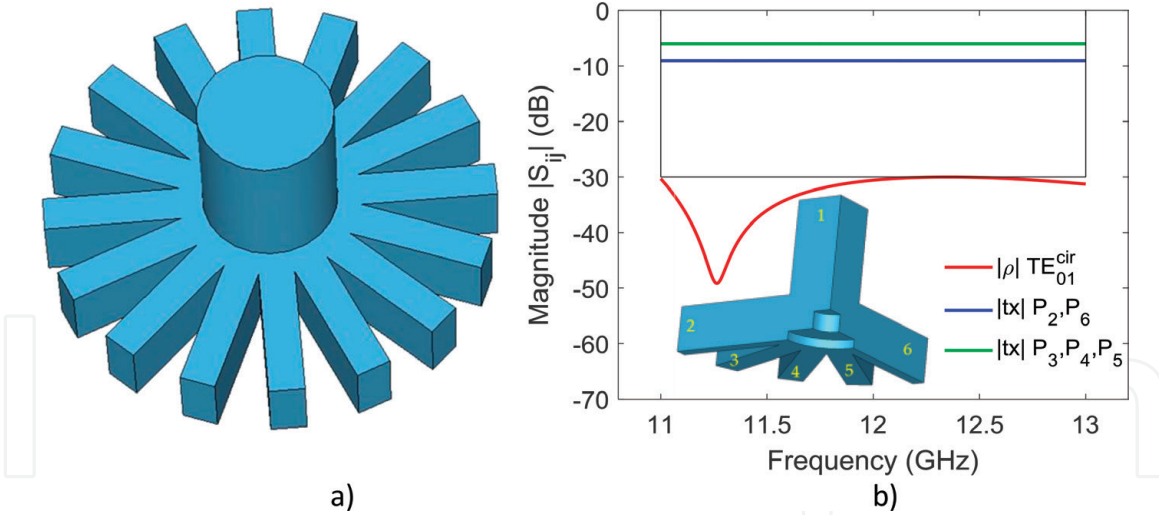
### 3. Design of the 16-way and 5-way power dividers

The circular waveguide  $TE_{01}$  mode generated by the transducer has to excite the radial divider, whose symmetry guarantees that the  $N$  output ports in **Figure 1** will have the same signal in amplitude and phase. Under the assumption that the radial divider will have low return loss, the power carried by the circular waveguide  $TE_{01}$  mode is equally divided in magnitude and phase into the  $TE_{10}$  mode of the  $N$  rectangular waveguides at the output ports. The radial dividers have typically a metallic post (with one or more sections) at the bottom of the structure. However, since the number  $N$  of output ports for the Ku- and W-band designs is very different (16 versus 5, respectively), additional strategies have been followed in each design for obtaining the specified challenging return loss level.

#### 3.1 16-way radial divider

In the case of a large number of ports, as in the 16-way power divider in the Ku-band, reduced height rectangular waveguides are typically connected to the base of the radial divider [11, 12]. Since the ports are implemented in standard waveguides, in this case  $N$  stepped transformers (normally only changing the height) would be required between the output ports and the circular cylinder of the divider. Therefore, the complexity, the size and the insertion losses would be increased. The design shown in **Figure 6a** avoids these transformers, with standard WR75 waveguides directly attached to the divider base. Therefore, even though 16 output waveguide ports are involved in the design, the radius of the base size is not enlarged. Since the height of the waveguide is not decreased, full power handling capability is maintained, and insertion losses are not degraded. In addition, 16 transformers are avoided, simplifying the manufacturing process and reducing the cost.

The radial symmetry with appropriate EW boundary conditions is also exploited in the simulations to reduce drastically the computation time. **Figure 6b** shows the

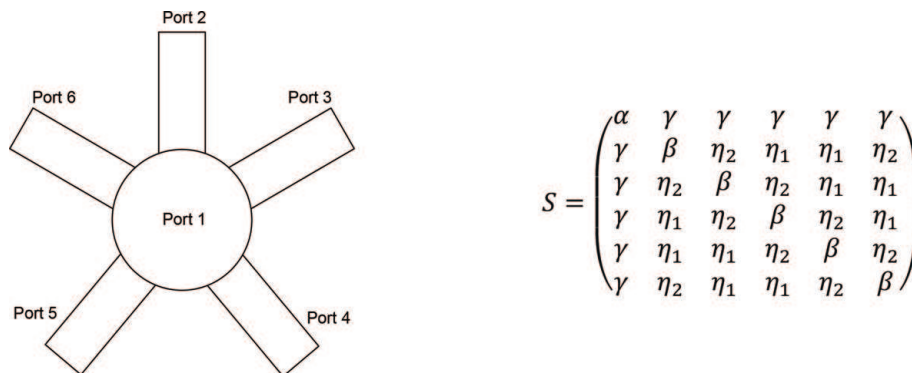

**Figure 6.**

(a) 3D CAD view of 16-way divider with the standard WR75 waveguides directly attached to the base without stepped transformers. (b) Simulated response of the reflection coefficient of the circular waveguide  $TE_{01}^{cir}$  mode, and the transmission to the  $TE_{10}^{rec}$  rectangular ports (from the  $TE_{01}^{cir}$ ), in the 16-way divider (only one quarter of the structure); in the inset, a 3D CAD view includes the port numbering.

theoretical full-wave simulated response of one quarter of the divider. The return loss level is better than 30 dB in the 2 GHz bandwidth. In the same figure, it can be seen the transmission coefficients corresponding to the simulation of one quarter of the whole structure. Thus, insertion loss in ports  $P_3$ ,  $P_4$  and  $P_5$  is 6 dB, but in ports  $P_2$  and  $P_6$ , with half-height, the level is 3 dB lower than in the other three, i.e., 9 dB (see the port numbering in the inset of **Figure 6b**). After this response is obtained, the 16-way power divider is ready to be connected to the transducer.

### 3.2 5-way radial divider

The ideal S-parameter matrix of a 5-way power divider is shown in (Eq. (1)), following the notation used in [33] (**Figure 7**). The coefficients  $\alpha$  and  $\beta$  represent the matching of the input and output ports, respectively. The coefficient  $\gamma$  is related to the input power division, while the coefficients  $\eta_1$  and  $\eta_2$  describe the coupling between pairs of different waveguide ports, two values in the case of  $N = 5$ . Assuming that the structure is lossless, the S-matrix is unitary and, consequently, it is possible to obtain the value of its elements, imposing perfect matching at the input port, i.e.,  $\alpha = 0$ . **Table 2** collects all the possible values for the other four elements (16 different matrices). It is interesting to note that in the case of  $N = 5$ , it is theoretically possible to match all the ports ( $\alpha = \beta = 0$ ).


**Figure 7.**

Scheme of a 5-way radial power combiner with port numbering according to (Eq. (1)).

$\gamma$	$\beta$	$\eta_1$	$\eta_2$	$\gamma$	$\beta$	$\eta_1$	$\eta_2$
$-\frac{\sqrt{5}}{5}$	$\frac{4}{5}$	$-\frac{1}{5}$	$-\frac{1}{5}$	$-\frac{\sqrt{5}}{5}$	0	$\frac{\sqrt{5}}{5}$	$-\frac{\sqrt{5}}{5}$
$\frac{\sqrt{5}}{5}$	$\frac{4}{5}$	$-\frac{1}{5}$	$-\frac{1}{5}$	$\frac{\sqrt{5}}{5}$	0	$\frac{\sqrt{5}}{5}$	$-\frac{\sqrt{5}}{5}$
$-\frac{\sqrt{5}}{5}$	$-\frac{4}{5}$	$\frac{1}{5}$	$\frac{1}{5}$	$-\frac{\sqrt{5}}{5}$	0	$-\frac{\sqrt{5}}{5}$	$\frac{\sqrt{5}}{5}$
$\frac{\sqrt{5}}{5}$	$-\frac{4}{5}$	$\frac{1}{5}$	$\frac{1}{5}$	$\frac{\sqrt{5}}{5}$	0	$-\frac{\sqrt{5}}{5}$	$\frac{\sqrt{5}}{5}$
$-\frac{\sqrt{5}j}{5}$	$\frac{4}{5}$	$-\frac{1}{5}$	$-\frac{1}{5}$	$-\frac{\sqrt{5}j}{5}$	0	$\frac{\sqrt{5}}{5}$	$-\frac{\sqrt{5}}{5}$
$\frac{\sqrt{5}j}{5}$	$\frac{4}{5}$	$-\frac{1}{5}$	$-\frac{1}{5}$	$\frac{\sqrt{5}j}{5}$	0	$\frac{\sqrt{5}}{5}$	$-\frac{\sqrt{5}}{5}$
$-\frac{\sqrt{5}j}{5}$	$-\frac{4}{5}$	$\frac{1}{5}$	$\frac{1}{5}$	$-\frac{\sqrt{5}j}{5}$	0	$-\frac{\sqrt{5}}{5}$	$\frac{\sqrt{5}}{5}$
$\frac{\sqrt{5}j}{5}$	$-\frac{4}{5}$	$\frac{1}{5}$	$\frac{1}{5}$	$\frac{\sqrt{5}j}{5}$	0	$-\frac{\sqrt{5}}{5}$	$\frac{\sqrt{5}}{5}$

**Table 2.**  
 All possible solutions for the S-matrix coefficients in an ideal 5-way radial divider.

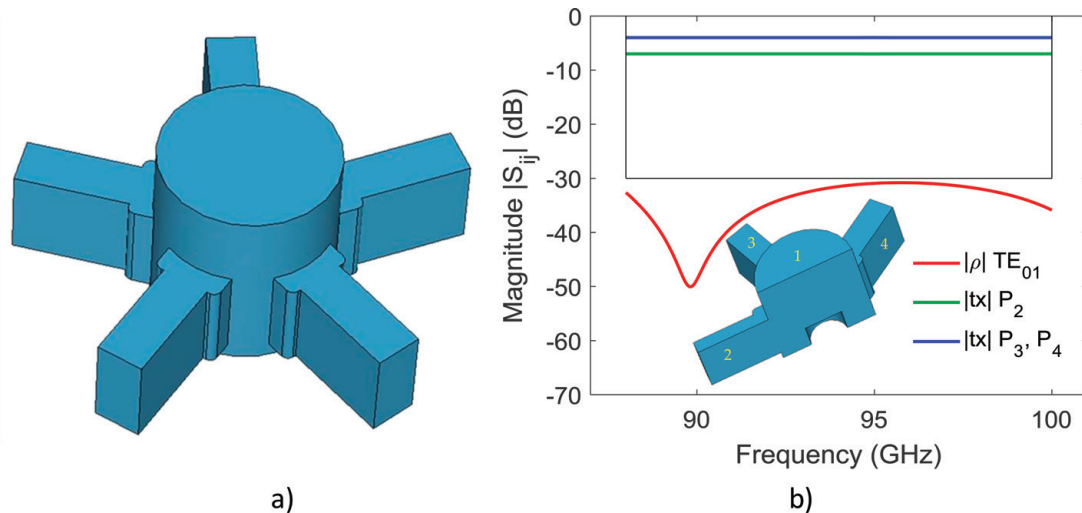


**Figure 8.**  
 (a) 3D CAD view of the 5-way divider. (b) Simulated response of the reflection coefficient for the circular waveguide  $TE_{01}^{cir}$  mode, and the transmission to the  $TE_{10}^{rec}$  rectangular ports (from  $TE_{01}^{cir}$ ) (only half of the structure); in the inset, a 3D CAD view including the port numbering is shown.

For our W-band design, the 5-way power divider implementation will follow the configuration shown in **Figure 8a**. In the full-wave simulations, the radial symmetry with appropriate EW boundary conditions is exploited to reduce the computation time. **Figure 8b** shows the theoretical full-wave simulated response of the divider. The return loss level is better than 30 dB in the 12 GHz bandwidth. Since the simulation has been done over one half of the structure, the insertion loss for ports  $P_3, P_4$  is 4.77 dB. In port  $P_2$ , with half-height, the level is 3 dB lower than in the others three, i.e., 7.77 dB (see the port numbering in the inset of **Figure 8b**).

#### 4. Integration of the transducer with the divider: experimental results of the Ku-band and W-band power combiners

The last step in the design is the integration of the mode transducer and the radial divider. Since the return loss levels in both components have been carefully



controlled, the final optimization of the full power combiner is a simple task only involving a few parameters: the radius of the circular waveguide and the dimensions of the matching cylinders in the divider and in the transducer. After that, the power combiners are manufactured and tested.

#### 4.1 Experimental results of the Ku-band power combiner

The 16-way radial Ku-band power combiner has been manufactured in brass. **Figure 9a** shows a photograph of the unit during the experimental characterization of the scattering parameters. In the photograph of **Figure 9a**, the combiner has 16 high-precision WR75 matched loads attached to its output ports. The manufacturing has been done in four parts, two halves corresponding to the mode transducer and another two halves corresponding to the radial divider. The cuts separating the parts have been done along the E-plane of the waveguides, in order to reduce the insertion losses.

**Figure 9b** shows the comparison between the simulation and the measurement of the return loss level, under excitation by the input common port. In the inset, the port numbering has been included in a 3D CAD view. The agreement between theory and simulation is excellent, even when the measured value is better than 30 dB in the 11–13 GHz bandwidth. Only a small difference is shown at the upper extreme of the band at 13 GHz.

**Figure 10a** presents the measured insertion loss of the 16-way combiner compared with i) the theoretical value assuming perfect conductor ( $\sigma = \infty$ ,  $-12.04$  dB), and ii) the average value simulated corresponding to the brass conductivity ( $\sigma = 15.9 \cdot 10^6$  S/m,  $-12.15$  dB). From these results, it can be said that the effective conductivity obtained in the manufacturing has virtually achieved the nominal value. The amplitude balance is also very good, since the extreme values are within  $\pm 0.15$  dB. The phase responses of the transmission from the input to the 16 output ports are shown in **Figure 10b**, with a detail in the inset. The balance between the extreme values is very good as well, within  $\pm 2.5^\circ$ .

**Figure 11a** shows the transmission between two output ports to characterize the isolation. One of the output ports has been selected, the sixth in this case, according to the inset in **Figure 9b**, which represents a generic case because of the rotational

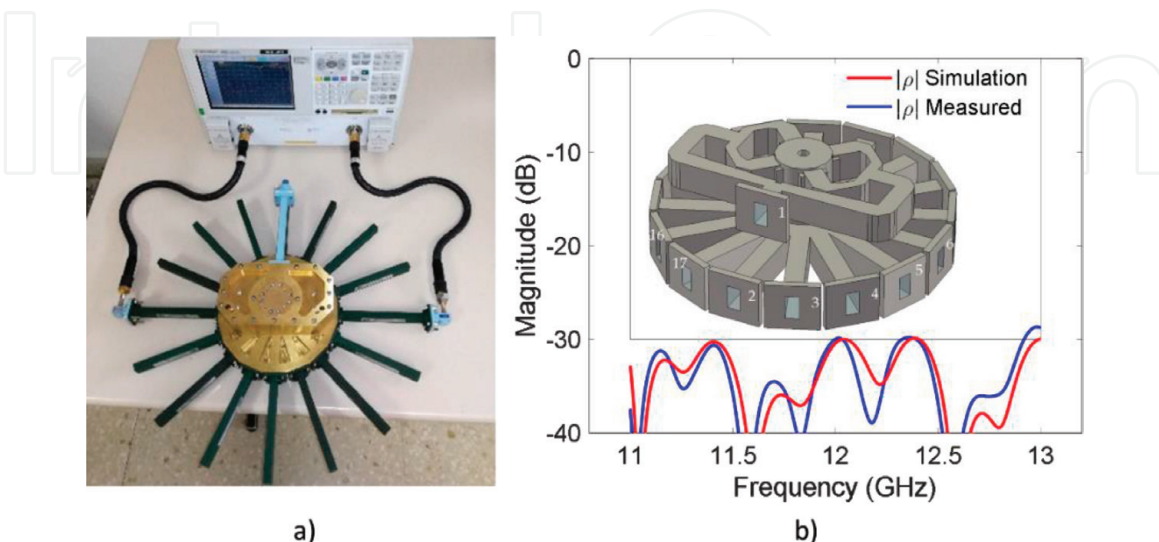


**Figure 9.** (a) Manufactured Ku-band prototype in the test bench including the high-precision matched loads in the output ports for the experimental testing. (b) Comparison between the simulation and the measurement of the return loss at the input (port 1 in the figure). In the inset, a 3D CAD view shows the port numbers.

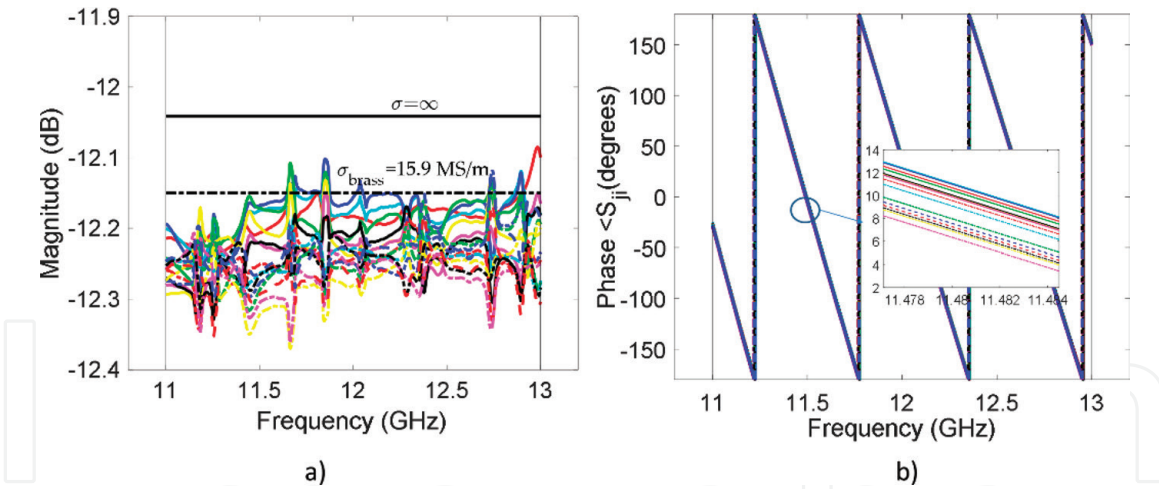


**Figure 10.** (a) Measured insertion loss of the 16-way Ku-band combiner compared with the theoretic value assuming perfect conductor ( $\sigma = \infty$ ,  $-12.04$  dB), and the average value simulated corresponding to the brass conductivity ( $\sigma_{brass} = 15.9$  MS/m,  $-12.15$  dB). (b) Measured phases of the 16-way combiner from port 1 to ports 2–17, with a detail in the inset.

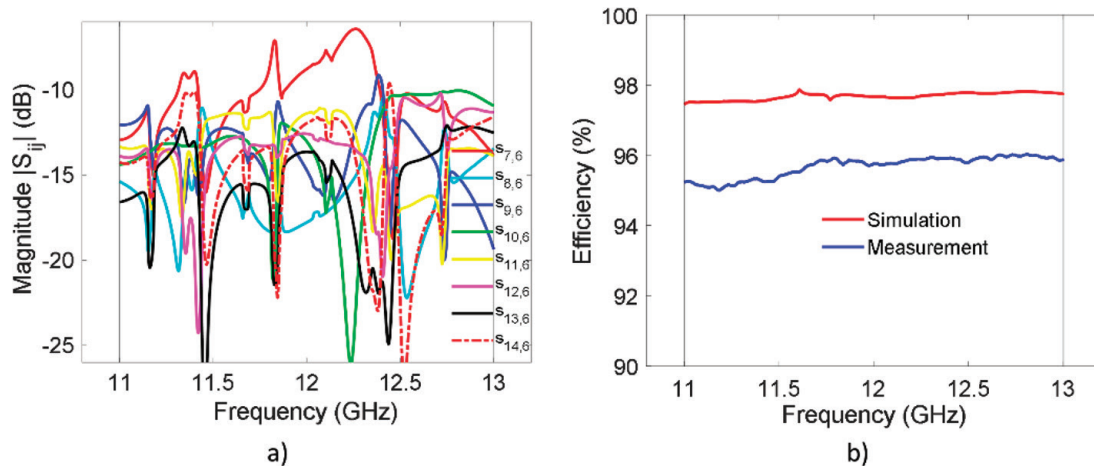


**Figure 11.** (a) Measured isolation response of the 16-way Ku-band power combiner: Transmission between the output port 6 (see the inset in Figure 9b) and the adjacent output ports of a middle of the combiner, i.e., the  $S_{7,6}$ ,  $S_{8,6}$ , etc. until  $S_{14,6}$  parameter. (b) Comparison between the simulated and measured combining efficiency.

symmetry. The graph shows the measured transmission to the adjacent ports:  $S_{7,6}$ ,  $S_{8,6}$ , etc., until the  $S_{14,6}$  parameter. The results for the other parameters related to the other half of the divider would be similar (the simulated results would be exactly equal for a perfectly symmetric combiner). The average value for these eight responses is approximately  $-14$  dB. However, it is interesting to note that the worst case corresponds to the isolation between two contiguous ports, the  $S_{7,6}$  parameter in this case, where the minimum value is close to  $-6$  dB.

In power combiners, a key figure of merit is the combining efficiency parameter [34], defined in (Eq. (2)), using the number 1 for the input common port. It characterizes the combined effect of the deviations of both magnitude and phase with respect to the ideal behavior. **Figure 11b** shows the simulated and measured efficiency, which is better than 95% in the whole operating bandwidth.

$$\xi = \frac{1}{N} \left| \sum_{k=1}^N S_{k+1,1} \right|^2 \quad (1)$$

## 4.2 Experimental results of the W-band power combiner

The 5-way radial W-band power combiner has been also manufactured in brass [16] by micromachining. The unit has been divided into four parts, which will be stacked vertically. **Figure 12a** shows the CAD view of the parts separated before the assembly, and also after the integration. **Figure 12b** shows a photograph of the combiner during the experimental characterization of the scattering parameters, with high-precision WR10 matched loads.

The comparison between the simulation and the measurement of the return loss level is shown in **Figure 13a**. This is the reflection coefficient seen at the input common port, which is port 6 in the numbering in the inset of the figure. The measured level is better than 20 dB in the complete operation band (12 GHz centered at 94 GHz), and better than 25 dB in the 80% of this bandwidth. These measured levels are coherent with the sensitivity analysis of the power divider taking into account a tolerance for the fabrication of  $\pm 0.02$  mm.

A systematic process has been followed to characterize the insertion loss of all the transmissions between the common input and the five outputs. According to

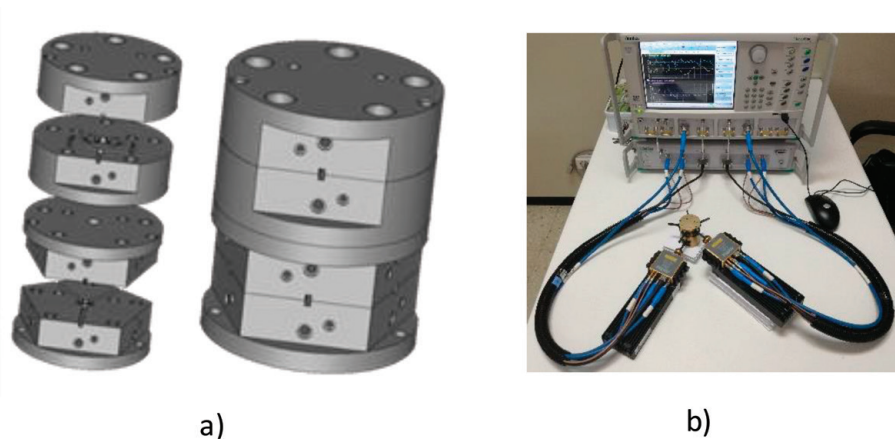


**Figure 12.**

(a) 3D CAD of the four sections in E-plane configuration to make the 5-way W-band combiner and its final assembly. (b) Manufactured prototype in the measurement bench including the high-precision matched loads in the output ports for the experimental characterization.

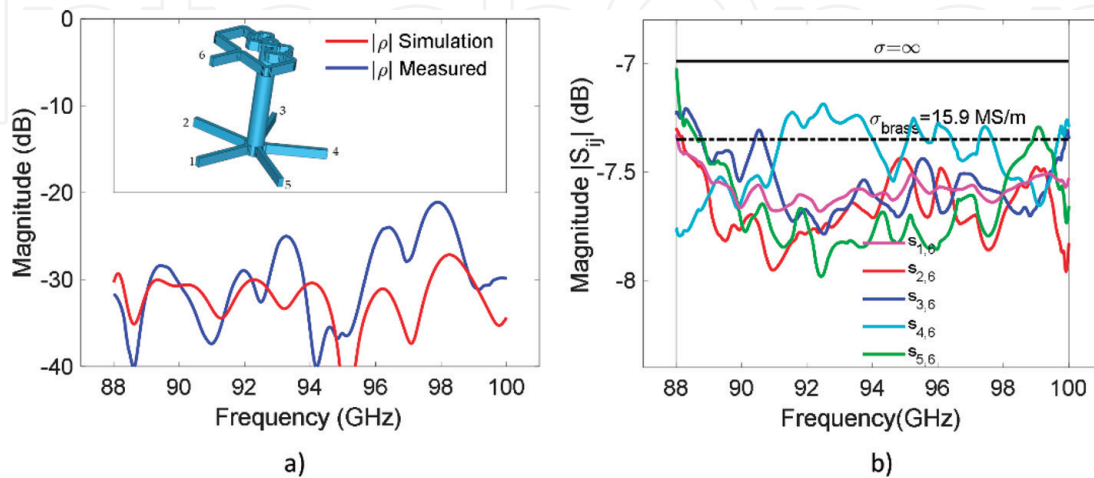


**Figure 13.**

(a) Comparison between the simulation and the measurement corresponding to the return loss level of the 5-way power combiner excited by the input common port (port 6 in the figure). In the inset a 3D CAD view is shown including the port numbers. (b) Measured insertion loss of the 5-way combiner compared with the theoretical value assuming perfect conductor ( $\sigma = \infty$ ,  $-6.99$  dB), and the average value simulated corresponding to the brass conductivity ( $\sigma_{\text{brass}} = 15.9$  MS/m,  $-7.35$  dB).



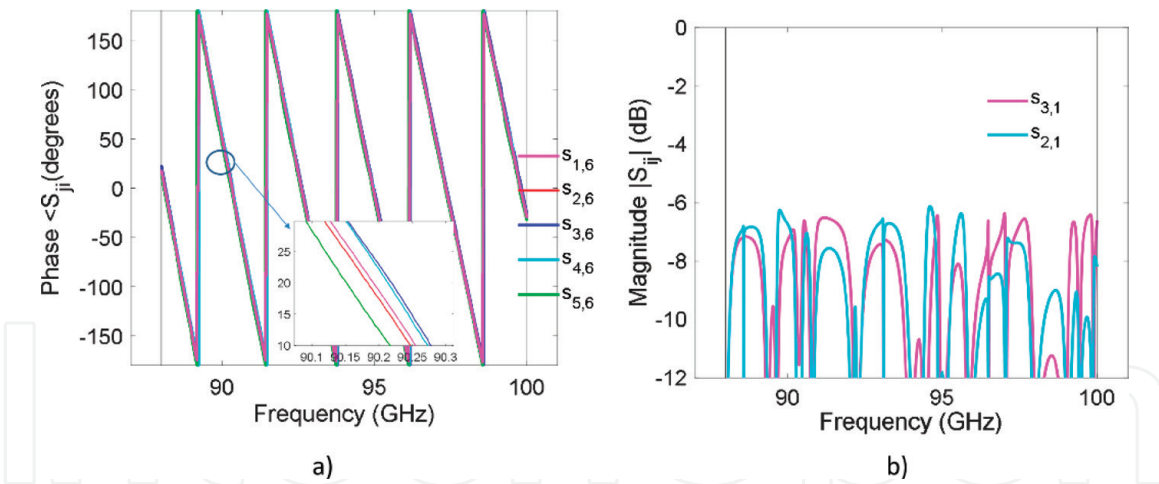


**Figure 14.** (a) Measured phases of the 5-way combiner, with a detail in the inset showing its very small difference. (b) Measured isolation response corresponding to the transmission between output port 1 (see the inset in **Figure 13a**), and the adjacent output ports of a middle of the combiner, i.e., the  $S_{2,1}$  and  $S_{3,1}$  parameters.

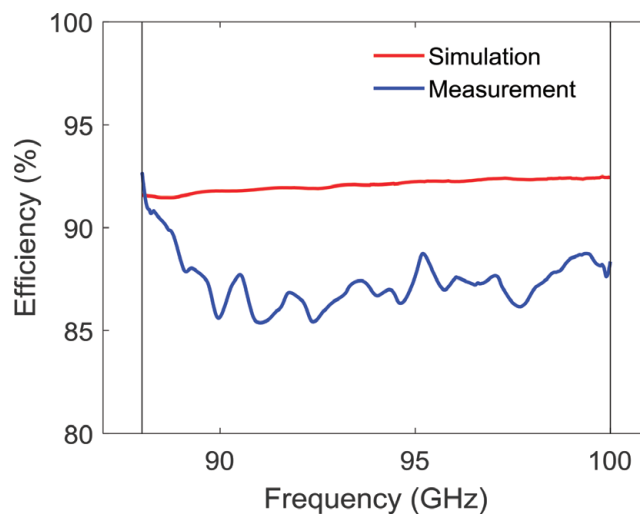


**Figure 15.** Comparison between the simulated and measured combining efficiency of the 5-way W-band power radial combiner.

the numbering in the inset of **Figure 13a**, the vector network analyzer is connected between port 6 and the corresponding port from 1 to 5, while the other four ports are connected to high precision matched loads (i.e., with return loss level better than 40 dB at W-band).

**Figure 13b** presents the measured insertion loss of the 5-way combiner compared with the theoretical value assuming perfect conductor ( $\sigma = \infty$ ,  $-6.99$  dB), and the average value simulated corresponding to the brass conductivity ( $\sigma_{\text{brass}} = 15.9 \cdot 10^6$  S/m,  $-7.35$  dB). The average measured value of  $-7.6$  dB implies that the effective conductivity obtained in the manufacturing is only slightly degraded with respect to the nominal value. The balance for the amplitudes is very good, since it is within  $\pm 0.4$  dB at the extremes of the band.

The phase response of the transmission between the input and the five output ports is shown in **Figure 14a**, with a difference at the extremes of the band within  $\pm 3.5^\circ$ , which also emphasizes the accurate manufacturing for obtaining this reduced margin at this band. **Figure 14b** shows the transmission between two output ports to characterize the isolation. Since the structure is symmetric, a generic port is selected (number 1 in this case, using the numbering in the inset of **Figure 13a**). In consequence, it is simulated and measured the transmission to its adjacent ports,



i.e., the  $S_{2,1}$  and  $S_{3,1}$  parameter. Their average level is approximately  $-7$  dB, very close to the theoretical value of  $|\eta_1| = |\eta_2| = |\sqrt{5/5}|$  in **Table 2**, which is  $-6.98$  dB. Finally, the efficiency has been simulated and measured showing both results in **Figure 15**. The measured efficiency is better than 85% in the whole operating bandwidth.

## 5. Conclusions

Two radial power combiners based on the  $TE_{01}$  mode of the circular waveguide have been designed, manufactured, and tested. They can be used in high-frequency systems for diverse applications at microwave and millimeter wave bands. A systematic step-by-step process has been followed to control the partial responses of the two main building blocks of the combiner, i.e., the mode transducer and the radial divider. In all the steps, the symmetry of each building block has been taken into account to reduce the computational effort in the optimization process. Moreover, the geometries have been simplified as much as possible to ease the manufacturing and to reduce the cost.

For the mode transducers, a strict control of the modes in the problem has been done by means of a rigorous analysis of the symmetry planes and the mode families involved in the structures. The sidewall excitation has led to very compact structures, which can also be used for mode transduction in other fields such as plasma heating.

In the case of the Ku-band 16-way divider, the output waveguides are directly connected to the divider without increasing the radius of the cylinder, avoiding extra stepped transformers. This improves the power handling and simplifies the manufacturing with respect to other designs using reduced height waveguides. In the case of the W-band 5-way divider, a careful design and the manufacturing by means of high precision micromachining with stacked waveguides have led to an excellent experimental performance.

The experimental results in both Ku- and W-bands are, to the authors' knowledge, the state-of-art of radial combiners based on the  $TE_{01}$  mode of the circular waveguide. This statement is based on the obtained results in return and insertion loss, and balance for both the phase and the amplitude. The Ku-band 16-way divider power combiner has achieved a 95% measured efficiency in a 16.7% fractional bandwidth. The W-band 5-way divider power combiner shows an 85% measured efficiency in a 12.8% fractional bandwidth.

## Acknowledgements

This work was supported by the Spanish government (Agencia Estatal de Investigación) under grants (ADDMATE) TEC2016-76070-C3-1/2-R (AEI/FEDER/UE) and the program of Comunidad de Madrid S2013/ICE-3000 (SPADERADARCM).

The authors would like to thank INMEPRE S.A., the diligence in the manufacturing.

IntechOpen

### **Author details**


José R. Montejo-Garai<sup>1\*</sup>, Jorge A. Ruiz-Cruz<sup>2</sup> and Jesús M. Rebollar<sup>1</sup>

<sup>1</sup> Grupo de Electromagnetismo Aplicado, Information Processing and Telecommunications Center, Universidad Politécnica de Madrid, Madrid, Spain

<sup>2</sup> Escuela Politécnica Superior, Universidad Autónoma de Madrid, Madrid, Spain

\*Address all correspondence to: [jr@etc.upm.es](mailto:jr@etc.upm.es)

### **IntechOpen**

© 2019 The Author(s). Licensee IntechOpen. This chapter is distributed under the terms of the Creative Commons Attribution License (<http://creativecommons.org/licenses/by/3.0>), which permits unrestricted use, distribution, and reproduction in any medium, provided the original work is properly cited. 

## References

- [1] Khan P, Epp L, Silva A. A Ka-band wide-bandgap solid-state power amplifier: Architecture performance estimates. IPN Progress Report 42-164. 2005;**42**:163
- [2] Kanto K, Satomi A, Asahi Y, Kashiwabara Y, Matsushita K, Takagi K. An X-band 250W solid-state power amplifier using gain power HEMTS. In: 2008 IEEE Radio and Wireless Symposium. 2008. pp. 77-80
- [3] Schellenberg J, Watkins E, Micovic M, Kim B, Han K. W-band, 5W solid-state power amplifier/combiner. In: 2010 IEEE MTT-S International Microwave Symposium Digest (MTT). 2010. pp. 240-243
- [4] Qiu JX, Levush B, Pasour J, Katz A, Armstrong CM, Whaley DR, et al. Vacuum tube amplifiers. IEEE Microwave Magazine. 2009;**10**(7):38-51
- [5] Epp LW, Hoppe DJ, Khan AR, Stride SL. A high power Ka-band (31-36 GHz) solid-state amplifier based on low-loss corporate waveguide combining. IEEE Transactions on Microwave Theory and Techniques. 2008;**56**(8):1899-1908
- [6] Russell KJ. Microwave power combining techniques. IEEE Transactions on Microwave Theory and Techniques. 1979;**27**(5):472-478
- [7] Chang K, Sun C. Millimeter-wave power-combining techniques. IEEE Transactions on Microwave Theory and Techniques. 1983;**31**:91-107
- [8] Montejo-Garai JR, Leal-Sevillano CA, Ruiz-Cruz JA, Rebollar JM, Estrada T. Synthesis and design of waveguide band-stop filters without out-of-band spurious responses for plasma diagnosis. Fusion Engineering and Design. 2012;**89**(9):1662-1666
- [9] Hsu T-I, Simonutti MD. A wideband 60 GHz 16-way power divider/combiner network. IEEE MTT-S International Microwave Symposium Digest. 1984, 1984;**1984**:175-177
- [10] Chen M. A 19-way isolated power divider via the TE<sub>01</sub> circular waveguide mode transition. In: 1986 IEEE MTT-S International Microwave Symposium Digest. 1986. pp. 511-513
- [11] Epp L, Khan P, Silva A. Ka-band wide-bandgap solid-state power amplifier: Hardware validation. IPN Progress Report. 2005;**42-163**
- [12] Chu Q-X, Mo D-Y, Wu Q-S. An isolated radial power divider via circular waveguide-mode transducer. IEEE Transactions on Microwave Theory and Techniques. 2015;**63**(12):3988-3996
- [13] Montejo-Garai JR, Saracho-Pantoja IO, Ruiz-Cruz JA, Rebollar JM. High-performance 16-way Ku-band radial power combiner based on the TE<sub>01</sub>-circular waveguide mode. Review of Scientific Instruments. 2018;**89**:034703
- [14] Zhang F, Song K, Li G, Zhao M. Sub-THz four-way waveguide power combiner with low insertion loss. International Journal of Infrared and Millimeter Waves. 2014;**35**:451-457
- [15] Zhang F, Song K, Fan M, Fan Y. All-metal-waveguide power divider with high power-combining efficiency. International Journal of Infrared and Millimeter Waves. 2016;**37**:258-266
- [16] Montejo-Garai JR, Ruiz-Cruz JA, Rebollar JM. 5-way radial power combiner at W-band by stacked waveguide micromachining. Nuclear Instruments and Methods in Physics Research Section A: Accelerators, Spectrometers, Detectors and Associated Equipment. 2018;**905**:91-95
- [17] Khan P, Epp L. Ka-band wide-bandgap solid-state power amplifier:

Prototype combiner spurious mode suppression and power constraints. IPN Progress Report. 2006;**42-163**

[18] Southworth G. Principles and Applications of Waveguide Transmission. The Bell Telephone Laboratories Series. Van Nostrand; 1956

[19] Leal-Sevillano CA, Ruiz-Cruz JA, Montejo-Garai JR, Rebollar JM. Field propagation in circular hollow waveguides with non-ideal metallic conductors from microwaves to terahertz frequencies. IEEE Transactions on Microwave Theory and Techniques. 2011;**59**(12):3013-3022

[20] Chu K. The electron cyclotron maser. Reviews of Modern Physics. 2004;**76**(2):489

[21] Blank M, Danly BG, Levush B. Experimental demonstration of a W-band (94 GHz) gyrotron amplifier. IEEE Transactions on Plasma Science. 1999;**27**(2):405-411

[22] Leou K, McDermott D, Balkcum A, Luhmann N. Stable high-power TE<sub>01</sub> gyro-twt amplifiers. IEEE Transactions on Plasma Science. 1994;**22**(5):585-592

[23] Garven M, Calame JP, Danly BG, Nguyen KT, Levush B, Wood F, et al. A gyrotron-traveling-wave tube amplifier experiment with a ceramic loaded interaction region. IEEE Transactions on Plasma Science. 2002;**30**(3):885-893

[24] Wolfert P. A wide-band rectangular-to-circular mode transducer for millimetre waves (correspondence). IEEE Transactions on Microwave Theory and Techniques. 1963;**11**(5):430-431

[25] Marie G. British Patent 805519; Dec 1958

[26] Saad S, Davies J, Davies O. Analysis and design of a circular TE<sub>01</sub> mode

transducer. IEE Journal on Microwaves, Optics and Acoustics. 1977;**1**(2):58-62

[27] Xue Q-Z, Zhang S-C, Liu P-K. Design of the H<sub>10</sub> to H<sub>01</sub> sector-type mode converter at Ka-band. International Journal of Infrared and Millimeter Waves. 2005;**26**(10):1407-1415

[28] Nusinovich G, Barker R, Luhmann N, Booske J. Modern microwave and millimetre-wave power electronics. 2005. Chapter 11

[29] Hoag H, Tantawi S, Callin R, Deruyter H, Farkas Z, Ko K, et al. Flower-petal mode converter for NLC. In: Particle Accelerator Conference Proceedings of the IEEE. 1993. pp. 1121-1123

[30] Yu C-F, Chang T-H. High-performance circular TE<sub>01</sub>-mode converter. IEEE Transactions on Microwave Theory and Techniques. 2005;**53**(12):3794-3798

[31] Montejo-Garai JR, Saracho-Pantoja IO, Ruiz-Cruz JA, Rebollar JM. Broadband and high-purity Ku-band circular TE<sub>01</sub>-mode converter. In: 2016 Asia-Pacific Microwave Conference (APMC). 2016. pp. 1-4

[32] CST, Computer Simulation Technology. Available from: <https://www.cst.com/>

[33] Holzman EL. An eigenvalue equation analysis of a symmetrical coax line to N-way waveguide power divider. IEEE Transactions on Microwave Theory and Techniques. 1994;**42**(1):1162-1166

[34] Gupta MS. Power combining efficiency and its optimisation. Proceedings of the Institute of Electrical and Electronics Engineers: Microwaves, Antennas & Propagation. 1992;**139**(3, pt. H):233-238